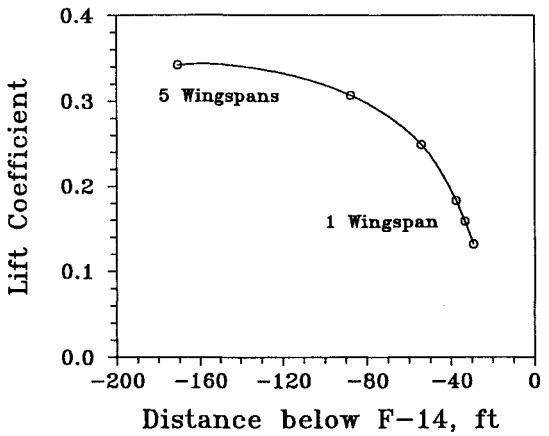

Fig. 3 Change in lift of T-34 because of vertical closure on F-14.

changes to be necessary for approaches to within a wingspan of the F-14.

A second effect of the aerodynamic interference of the F-14 on the T-34, besides the change in the local flowfield direction in the tail region, is the increased pressure in the vicinity of the underside of the F-14. The increased pressure flowfield results in higher pressures on the upper or suction side of the wing of the T-34, and accordingly a loss in lift, as shown in Fig. 3. The T-34 loses approximately 55% of its lift when it is one wingspan away from the larger aircraft and 90% of its lift when a semispan away. To the pilot, this loss of lift can correspond to a sensation of being pushed away by the F-14. Conflicting cues of loss of lift and a nose-up rotation may be disorienting to the pilot unfamiliar with closing on a dissimilar aircraft. As noted earlier, the pitch angle of the T-34 was held constant for all test cases. The pilot would actually expect nose-up trim to be necessary to regain the lift as the larger aircraft was approached. The nose-up rotation is ironically supported by the pitch-up tendency; an enhanced awareness of the two responses and their interaction is necessary on the part of the pilot when closing on a dissimilar aircraft.

Concluding Remarks

This Note has indicated the flowfield effects of mutual interference for only one scenario; it is not intended to be a primer on formation flying. The closure position considered of the T-34 beneath the F-14 may be one of the most unsafe positions possible for approaching another aircraft. The natural tendency as the pilot looks up to the belly of the F-14 will be to pull back on the stick, increasing the closure rate. Because of the proximity of the leading aircraft, visual cues used to judge closure are lacking, and even an alert pilot will have difficulty recognizing vertical closure rates. Formation flying requires skills learned in specific training, which includes an understanding of the responsibilities of both leader and wingman.

Acknowledgments

This project was funded by the Naval Air Systems Command, AIR-53011C, with Jonah Ottensoser as the Technical Monitor. The authors are grateful for the support. The authors also appreciate the helpful comments of the reviewer, a retired military instructor pilot, and those offered by pilot students at the U.S. Naval Postgraduate School.

References

[1]Byrd, C., "Summary of Mid-Air Collisions During Formation Flight," Naval Safety Center, NSC Code 10, Feb. 1993.

[2]Perkins, J. R., "1982 to Date Mid-Air Collision Summary," Headquarters Air Force Safety Agency, HQ AFSA/SERD, Feb. 1993.

[3]Porter, D. B., and Howard, R. M., "Aerodynamic Interference Associated with Formation Flying," U.S. Naval Postgraduate School, Monterey, CA, Jan. 1995.

[4]Porter, D. B., and Howard, R. M., "Dissimilar Aircraft Flying in Close Proximity," U.S. Naval Postgraduate School, NPS-AA-95-001, Monterey, CA, Jan. 1995.

[5]Porter, D. B., "A Numerical Study of Airplanes Flying in Proximity," Masters Thesis, U.S. Naval Postgraduate School, Monterey, CA, Sept. 1993.

[6]Ashby, D. L., Dudley, M. R., Iguchi, S. K., Browne, L. and Katz, J., "Potential Flow Theory and Operation Guide for the Panel Code PMARC," NASA TM-102851, Jan. 1991.

Computational Analysis of a Wingtip-Mounted Pusher Turboprop

J. Mark Janus,* Animesh Chatterjee,† and Chris Cave†
Mississippi State University,
Mississippi State, Mississippi 39762

Nomenclature

C_L	=	configuration lift coefficient, lift/($q_\infty S_{ref}$)
q	=	dynamic pressure, (ρV^2)/2, lb/ft^2
S_{ref}	=	reference area (baseline wing exposed planform area), ft^2
V	=	flow velocity, ft/s
α	=	angle of attack, deg
$\beta_{3/4}$	=	three-quarter tip radius blade setting angle, deg
ξ, η, ζ	=	computational coordinates; axial, radial, and circumferential, respectively
ρ	=	flow density, slug/ft^3

Subscript

∞	=	freestream conditions

Introduction

THE aerospace community has had a long history investigating methods for the reduction of induced drag (drag due to lift of a finite wing).[1] Although induced drag is about 50% of the total drag for subsonic transport aircraft at cruise conditions, most of the recent innovative research in transport aircraft drag reduction has concentrated on skin-friction drag (i.e., laminar flow and turbulent-drag reduction schemes such as riblets). Increasing aspect ratio and tailoring the span-load distribution have been the designers' primary tools for minimizing induced drag. Though means have been found to minimize induced drag, it has long been accepted as a necessary by-product of generating lift on a finite span wing. However, induced drag is not essential for the production of lift, but only an adverse consequence of that process.

Results from wind-tunnel tests have indicated large reductions in induced drag for wings with tip-mounted engines.[2,3] The results of an exploratory investigation to determine the

Presented as Paper 93-0524 at the AIAA 31st Aerospace Sciences Meeting and Exhibit, Reno, NV, Jan. 11–14, 1993; received April 9, 1995; revision received Sept. 13, 1995; accepted for publication Sept. 13, 1995.

*Assistant Professor, National Science Foundation, Engineering Research Center for Computational Field Simulation, Department of Aerospace Engineering, P.O. Box 6176. Senior Member AIAA.

†Graduate Student, National Science Foundation, Engineering Research Center for Computational Field Simulation, Department of Aerospace Engineering, P.O. Box 6176. Student Member AIAA.

installed performance of a wingtip-mounted pusher turboprop were reported in Refs. 3 and 4. The design philosophy centered around vortex energy recovery and induced drag reduction. The anticipated result, favorable interference, was apparently borne out in the measured data. The configurations numerically simulated in this study are the same as those reported on in Ref. 3. Numerical simulations similar to that of the exploratory investigation were performed to corroborate the data obtained from that effort and to obtain insight into the performance enhancing mechanism(s) involved.

Solution Technique

The objective of this effort was to model the formation of the tip vortex and simulate its interaction with a tip-mounted turboprop engine. The application of a Euler method was considered a logical first step towards the flow analysis of the configurations studied here. Although the angle-of-attack range studied is very low, the effect of neglecting viscous effects on the predicted flowfield is unknown. To adequately correlate the relationship between angle of attack and interference effects, several numerical simulations (at differing inflow angles) were necessary. Data collected from the numerical simulations included aerodynamic force coefficients, propeller performance coefficients, and flowfield maps.

The flow model used in the simulations, the details of which can be found in Refs. 5 and 6, solves the unsteady three-dimensional Euler equations, discretized as a finite volume method, utilizing a high-resolution approximate Riemann solver for cell interface flux definitions. The numerical scheme is an approximately factored, block lower–upper, implicit, Newton iterative-refinement method. Multiblock domain decomposition is used to partition the field into an ordered arrangement of blocks. Block–block relative motion is achieved using local grid distortion.

The baseline geometry, a fuselage–wing (FW) configuration, was a semispan model incorporating a fuselage with an unswept, untapered, untwisted wing. The wing had a chord of 13 in., an aspect ratio of 6.10 based on full wingspan of 79.26 in., and a NACA 64_1A012 airfoil section. The tip was modeled with a symmetrical cap. The fuselage–wing–nacelle–prop (FWNP) configuration, a derivative of this geometry with a tip-mounted nacelle and an SR-2 design high-speed propeller in a pusher configuration was also analyzed (see Fig. 1). The propeller consisted of eight blades with $\beta_{3/4} = 57.1$ deg. A third (intermediate) geometry, the fuselage–wing–nacelle (FWN) configuration, consisting of the fuselage–wing with the nacelle, but no blades, was also analyzed. The flow conditions were set to a Mach number of 0.70 and angles of attack ranging from approximately 0 to +5 deg. The tunnel Reynolds number for this geometry based on the wing chord was 3.82×10^6.

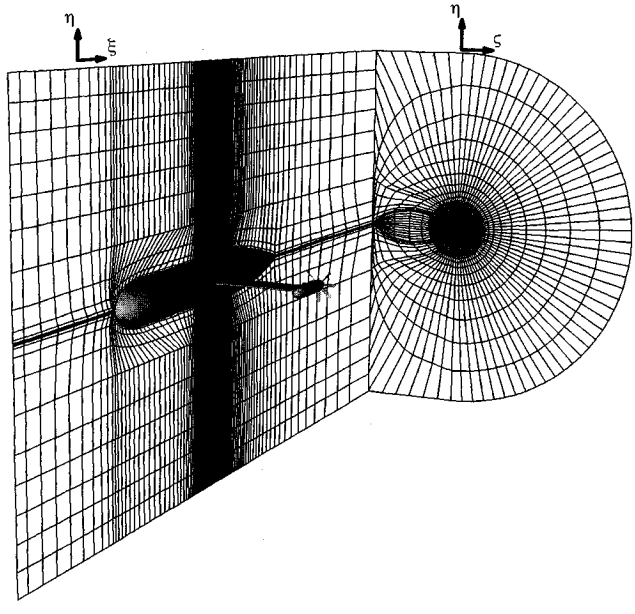

Fig. 1 Computational grid arrangement.

All of the steady flow cases were run using local time stepping at a Courant number of seven using a single Newton iteration with at least 2000 cycles of processing. The unsteady runs (FWNP) were executed as restarts from the FWN cases and processed for an additional 1440 time steps using minimum time stepping with a single Newton iteration for the first 960 and then five iterations for the remainder of the run. Physically this represents a total of 15 prop revolutions. The processing rate on a Cray Y-MP for each iteration of each time step was approximately 22,000 computational cells per second or (4.5×10^{-5} s/cell). The run schedule covered 0 to +5 deg incrementing by 1 deg for the steady runs and incrementing by 2 deg for the unsteady runs.

The data obtained from the schedule of runs included aerodynamic forces, turboprop performance, and flowfield maps. The aerodynamic force data were collected via surface pressure integration over configuration components. Because of the extreme difficulty of accurately accessing the drag coefficient using surface pressure,[7] drag calculations collected via surface pressure integration are not considered acceptable. Lift is much less susceptible to these inaccuracies, as shown in Ref. 7.

Results and Discussion

The variations in configuration lift coefficient with angle of attack (C_L vs α) for the FW, FWN, and FWNP configurations produced from the computational analysis are presented in Fig. 2. Note, as in Ref. 4, the reference area is taken to be the exposed area of the basic FW wing panel in all cases and not the actual planform area of each particular configuration. In this light, Fig. 2 actually represents data with a consistent nondimensionalization, i.e., normalized lift vs α. The simulated behavior follows the same trends (relative to the change in lift associated with a change in configuration) as that measured in the wind tunnel. From these plots it is seen that the computational results consistently underpredict the values obtained experimentally by about 10%. One explanation for the underprediction was the lack of wind-tunnel wall effects. Consider the corresponding plot for the FW and FWN cases with tunnel walls modeled (see Fig. 3). The tunnel walls improve the lifting characteristics of each body as compared to free flight, which is clearly borne out in these plots. Thus, reasonable agreement was obtained for configuration lift and presumably component lift values when the tunnel walls were included in the numerical simulation. Modeling the wind-tunnel walls requires generating a new grid for each angle of attack since the

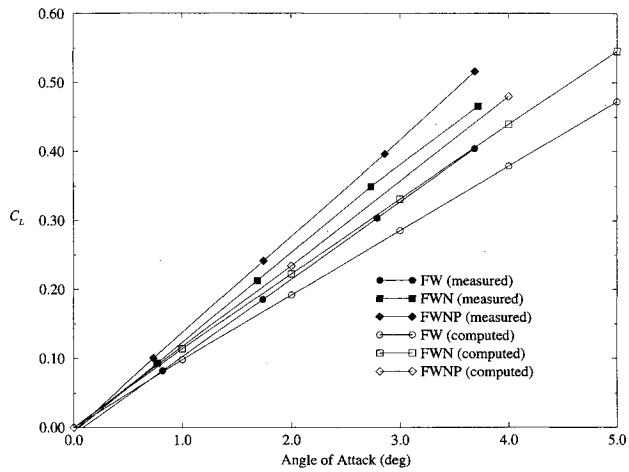

Fig. 2 Normalized lift vs angle of attack (free-flight simulation).

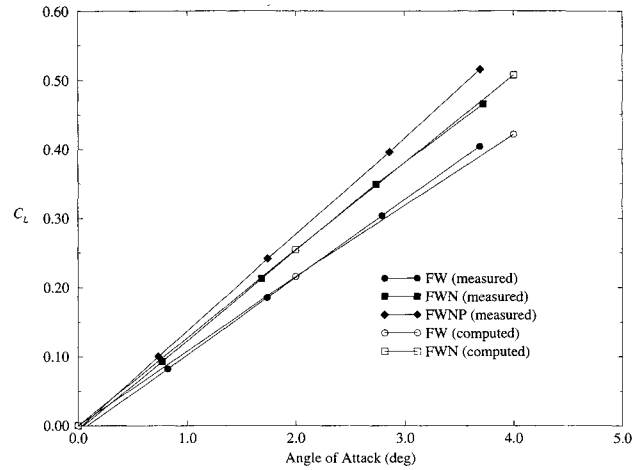

Fig. 3 Normalized lift vs angle of attack (tunnel wall simulation).

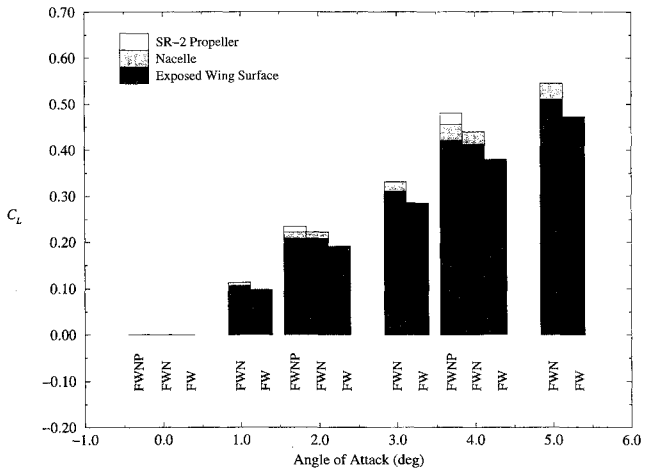

Fig. 4 Component lifting surface breakdown.

walls become part of the geometry. Because of this additional grid complexity and the apparent capture of the correct trends in Fig. 2, the isolation of the lift contribution from the various surfaces was performed simulating free flight.

A component breakdown of the lift resulting from the different configurations is given in Fig. 4. This was used to help determine the impact of major component surface loads resulting from configuration modifications in an effort to access possible reasons for the performance enhancement observed. The computational data indicate that the addition of the nacelle has a significant impact on the lift produced by the wing panel (which with the nacelle added is 7% shorter than the basic panel). At least part of this improved performance from the smaller wing panel should be considered as an alpha flow effect created by the nacelle at the junction to the wing.[8] The addition of the nacelle has increased the overall planform area roughly 15% and aspect ratio about 5%.

Focusing attention on the 4-deg case for the FWN configuration, the component lift because of the nacelle appears to account for roughly half of the total lift increase over that calculated for the basic panel. The propeller is another potential contributor to the overall lift of the FWNP configuration for the 4-deg case and is shown here to yield approximately 25% of the increment in lift over that of the basic panel. The nacelle provides nearly 35% of the increase, with the remaining 40% coming from the wing.

A pusher propeller mounted on a wingtip sees quite a varying inflow field. The advancing blade (blade passing outboard) is highly loaded because of the vortex flow from the wingtip and the geometric angle of attack of the wing itself. Operating in the wake of the wing, the retreating blade sees a much different inflow field and is more lightly loaded. Each blade's aerodynamic force component perpendicular to freestream will be transmitted back to the rest of the configuration through the propeller shaft as a lift force. The large contribution to the lift because of the propeller, shown in Fig. 4, is from the differential loading on the blades, biased in the positive lift direction.

This lift force would have also been present in the wind-tunnel data since the lift on the shaft was included in the forces measured by the main balance in the tunnel experiment. In addition, further accounting for lift has shown that the spinner (which was included in the nacelle increment here), brings the total increase because of rotating components to nearly 35%. This would explain the observation that the wing pitching moment about the midchord went from a positive value (pitchup) to essentially zero for the power-on case.[4] The stabilizing moment is likely because of the propeller and spinner lift. Additional experimental data involving a wingtip extension (increasing the wingspan by adding a section outboard of the engine) indicated no stabilizing moment present. This would be expected since a pusher propeller operating inboard of the wingtip experiences a flow straightening effect because of the wing for both the retreating and advancing blades and would not have a large differential blade loading. Without the differential blade loading, the additional lift force at the shaft would not be present to provide the pitchdown stabilizing moment.

Conclusions

A computational analysis of a family of configurations was performed. The potential for gaining a better understanding of the underlying physics behind the effective operation of a complex configuration such as a wingtip-mounted turboprop is encouraging. Good agreement with wind-tunnel data was obtained concerning configuration lift curves. The breakdown of component lifting surfaces indicated that the nacelle and propeller were significant sources of total configuration lift. Although it appears the induced effects on the wing are reduced due to the tip attachments, much of the improved (lifting) performance is attributable to surfaces other than the wing.

Acknowledgments

Funding for this project was provided by NASA Langley Research Grant NAG-1-1271 with Dennis Bartlett as the Technical Monitor. The authors would like to acknowledge David L. Whitfield and James C. Patterson, who throughout the course of this endeavor were extremely helpful. The authors would also like to thank Mississippi Center for Supercomputing Research for providing several hours of Cray time for project software debugging and a portion of the runs presented here.

References

[1]Henderson, W. P., and Holmes, B. J., "Induced Drag—Historical Perspective," Society of Automotive Engineers Technical Paper Series, SAE Aerotech '89 Conf., Sept. 1989.

[2]Patterson, J. C., Jr., and Flechner, S. G., "An Exploratory Wind-Tunnel Investigation of the Wake Effect of a Wing-Tip-Mounted Fan-Jet Engine on the Lift-Induced Vortex," NASA TND-5729, May 1970.

[3]Patterson, J. C., Jr., and Bartlett, G. R., "Effect of a Wing-Tip-Mounted Pusher Turboprop on the Aerodynamic Characteristics of a Semi-Span Wing," AIAA Paper 85-1347, July 1985.

[4]Patterson, J. C., Jr., and Bartlett, G. R., "Evaluation of Installed Performance of a Wing-Tip-Mounted Pusher Turboprop on a Semi-Span Wing," NASA TP 2739, Aug. 1987.

[5]Janus, J. M., "Advanced 3-D CFD Algorithm for Turbomachinery," Ph.D. Dissertation, Mississippi State Univ., Mississippi State, MS, May 1989.

[6]Horstman, H. Z., "Incorporation of Radial Partitioning in a Turbomachinery Flow Solver for Unsteady Ducted Applications," M.S. Thesis, Mississippi State Univ., Mississippi State, MS, Aug. 1991.

[7]Nikfetrat, K., Van Dam, C. P., Vijgen, P. M. H. W., and Chang, I. C., "Prediction of Drag at Subsonic and Transonic Speeds Using Euler Methods," AIAA Paper 92-0169, Jan. 1992.
[8]Hoerner, S. F., *Fluid-Dynamic Lift*, edited by H. V. Borst, Hoerner Fluid Dynamics, Brick Town, NJ, 1985, Chap. 19, p. 5; Chap. 20, p. 14.

Aircraft Concept Optimization Using Parametric Multiobjective Figures of Merit

Brett Malone* and W. H. Mason†
Virginia Polytechnic Institute and State University, Blacksburg, Virginia 24061

Introduction

THE difference between aircraft optimized for different figures of merit is of interest to aircraft designers, e.g., the contrast between a minimum takeoff gross weight design and a minimum fuel weight design. Results obtained using different single-objective figures of merit were compared by Jensen et al.[1] and Johnson.[2] The results from single figure of merit studies are useful, but do not give a clear picture of how a design changes as it moves from one figure of merit to another. By examining the evolution from one design to another, a deeper understanding of the role of the figure of merit can be gained. In this Note we extend our previous work[3] to handle several figures of merit through the use of a multiobjective figure of merit approach, and show how this approach can be used to gain additional insight into the relative importance of various figures of merit. Using this method, the evolution of an optimum design from one figure of merit to another is demonstrated. Specifically, we have used combinations of minimum takeoff gross weight, structural weight, fuel weight, maximum cruise performance, and productivity parameters as figures of merit.[4] We use the global sensitivity equation (GSE) approach, and computational speed is facilitated by the use of simple algebraic representations of the system technologies.

Global Sensitivity Approach and Algebraic Technology Representations

Sets of optimum designs for various figures of merit can be obtained quickly using the multidisciplinary methods developed by Sobieski,[5] and by taking advantage of the low computational time afforded by the use of algebraic expressions for various technology models. The approach is structured so that the algebraic models can be replaced by improved analysis as desired. An alternate, much more efficient approach to incorporation of more advanced analysis methods is possible using the variable-complexity approach.[6]

Presented as Paper 92-4221 at the AIAA Aircraft Design Systems and Operation Meeting, Hilton Head, SC, Aug. 24–26, 1992; received Jan. 23, 1995; revision received Nov. 12, 1995; accepted for publication Nov. 18, 1995.

*Research Associate, ACSYNT Institute. Student Member AIAA.
†Professor, Department of Aerospace and Ocean Engineering. Associate Fellow AIAA.

The GSE method is used to determine the interactions between the system technologies. The gradients of the figure of merit and constraints are available from the GSE analysis. The solution to the numerical optimization problem is obtained using a nonlinear quadratic programming algorithm[7] with the GSE gradients supplied for the search direction computation. Complete details of the method are given in Ref. 3.

Parametric Multiobjective Function Formulation

As described previously, we define a range of figures of merit for use in multiple optimization cases to illustrate the evolution of a design from one figure of merit to another. This is done by defining a multiobjective figure of merit F in the following manner:

$$F = K_0 F_{\text{obj1}} + (1 - K_0) F_{\text{obj2}} \tag{1}$$

where K_0 is a blending parameter that varies from 0 to 1. When $K_0 = 1$, the figure of merit is the first figure of merit F_{obj1}, and when $K_0 = 0$, the figure of merit is entirely F_{obj2}. When K_0 is between 1 and 0, the overall figure of merit is a combination of the two.

Illustrative Example

Baseline Mission and Design Variable Set

Our parametric multiobjective function approach is illustrated using a short takeoff, medium-range cargo transport. Table 1 gives the specified mission statement and constraints along with a definition of the propulsion system. In this example, the range and the engine thrust were fixed. The problem was studied previously in Ref. 3 for a single objective function.

The design variables were chosen to include both aircraft geometry and flight performance values. Seven design variables were chosen for optimization:

$$X = (\text{AR}, S_w, h, M, \Lambda, t/c, \lambda)^T \tag{2}$$

where AR is the aspect ratio, S_w is the wing area, h is the cruise altitude, M is the Mach number, Λ is the wing sweep angle, t/c is the wing thickness to chord ratio, and λ is the wing taper ratio. Variations in the optimum values of the design variables along with the figure of merit values will be examined as the parameter K_0 is varied. The results provide insight into how the aircraft geometry is affected by changing the figure of merit, and what combinations of these figures of merit result in the most robust aircraft design for various mission profiles.

Solutions for Minimizing Fuel Weight and Wing Weight

As an example, we select the cruise fuel weight and the wing structural weight as the two figures of merit to use in our multiobjective figure of merit. Other examples are given in Ref. 4. The formulation for the multiobjective function for this case is given by

$$F = K_0 W_{\text{wing}} + (1 - K_0) W_{\text{fuel}} \tag{3}$$

where W_{wing} is the wing weight, and W_{fuel} is the fuel weight. A takeoff constraint of 5000 ft is imposed along with a section

Table 1 Mission requirements/constraints

Cargo weight, 150,000 lb
Range, 3,000 nm
Takeoff distance, 5,000 ft
Landing distance, 4,000 ft
Maximum C_L, 2.3
Maximum section $C_{l\,\text{cruise}}$, 1.0
Propulsion, 4 CF6 class turbofans